MOLECULAR DYNAMICS OF TRYPTOPHAN IN RIBONUCLEASE-T1

I. Simulation Strategies and Fluorescence Anisotropy Decay

PAUL H. AXELSEN, CHRISTOPHER HAYDOCK, AND FRANKLYN G. PRENDERGAST
Department of Biochemistry and Molecular Biology, Mayo Clinic/Foundation, Rochester, Minnesota 55905

ABSTRACT Molecular dynamics simulations of Ribonuclease-T1 (RNAse-T1) were performed using x-ray crystal coordinates for the enzyme and various simulation strategies. From each of the simulations, a predicted fluorescence anisotropy decay for the single-tryptophan residue was derived and compared with experimental values for the limiting anisotropy of this protein. Simulations conducted in vacuo demonstrated large displacements among some of the residues adjacent to the tryptophan side chain. As a consequence, the ring system rotates relatively unhindered through an angle far in excess of that implied by experimental data. In contrast, the explicit simulation of solvent within a stochastic boundary led to excellent agreement between simulation and experiment. In the case of RNAse-T1, the experimentally-determined limiting anisotropy is useful as a criterion of simulation accuracy in the vicinity of the tryptophan side chain.

INTRODUCTION

Tryptophan (TRP) is a sensitive fluorescent probe of protein structure and dynamics. Yet, despite many analyses of TRP fluorescence in proteins, our understanding of the relationship between TRP fluorescence and its physicochemical environment is largely qualitative. Formidable hurdles, both theoretical and technical, have impeded progress in this field. For example, any quantitative explanation of fluorescence lifetime, quantum yield, or the wavelength characteristics of absorption and emission dipoles must await development of a satisfactory theory which describes the excited states of indole. Anisotropy decay and susceptibility to quenching are perhaps better understood theoretically, but such phenomena are governed by protein conformational fluctuations in the picosecond time domain. Until recently, direct experimental observations of events on a picosecond time scale have not been feasible and detailed simulations of protein dynamics could not be quantitatively correlated. The recent development of instruments capable of measuring fluorescence anisotropy decay with picosecond time resolution (Lakowicz et al., 1987) impels us to further develop theory concerning fluorophore dynamics in protein.

The series of proteins with a single TRP residue and known x-ray crystal structure are invaluable to research in this area. The interpretation of fluorescence signals from such proteins is vastly simplified, although better still would be a protein devoid of all other aromatic residues. Among this series of proteins, ribonuclease T1 (RNAse-T1) is of particular interest due to its unusual spectral properties.

The limiting anisotropy of TRP (fluorescence in RNAse-T1, $r(o)$,[1] is nearly equivalent to that of simple indole compounds in vitrified solution (Lakowicz et al., 1983; Eftink, 1983). This implies that very little motion of the fluorophore occurs within the protein and hence, interatomic distances between the fluorophore and its protein environment are relatively fixed. The high quantum yield of this fluorophore and the presence of vibrational structure (albeit, poorly resolved) in its emission spectrum (James et al., 1985) are characteristic of indole compounds in nonpolar solvents. However, the emission spectrum is blue shifted relative to TRP fluorescence in most proteins and is red shifted relative to indole compounds in nonpolar solvents such as cyclohexane (Creed, 1984). Therefore, while this residue may be largely sequestered from solvent, it remains spectrally perturbed by some feature of its protein environment. Finally, the fluorescence intensity decay of TRP-59 is clearly pH dependent, with single exponential decays observed at pH <6.0 and biexponential decays detected at pH >7.0 (Chen et al.,

Please address all correspondence to Franklyn Prendergast.

[1]We distinguish between r_o and $r(o)$, the former being the anisotropy of fluorescence at time = 0 such as would be measured in a vitrified solvent, the latter being the anisotropy as a function of fluorescence lifetime, τ, in the limit $\tau \rightarrow 0$. In practice, $r(o) \leq r_o$.

1987; Eftink and Ghiron, 1987). Taken together, these features suggested to us that a meaningful correlation may be demonstrated between these experimental observables and simulated molecular dynamics trajectories.

Computer simulations of macromolecular dynamics have been performed for over ten years as of this writing. Programs such as CHARMM (Brooks et al., 1983), generally implement systems of semi-empirical forces, fixed charges, and immutable connectivities. Atoms are propagated according to classical equations of motion and quantum mechanical effects are not explicitly considered. Ichiye and Karplus (1983), using CHARMM, have rigorously detailed the derivation of fluorescence anisotropy decay from these trajectories.

Molecular dynamics simulations have enormous memory and computational power requirements, forcing consideration of various problem-size reduction strategies. For example, these simulations are often conducted with a single protein in the absence of solvent, a so-called vacuum simulation. This approach has been accorded greater validity when the region of interest lies buried within the protein matrix (van Gunsteren and Karplus, 1982). Brooks and Karplus (1986) have reviewed various methods of simulating protein dynamics under solvated conditions, including one in which solvent is incorporated along with a small region of interest into a stochastic boundary (Berkowitz and McCammon, 1982; Brünger et al., 1984; Brooks et al., 1985). As an alternative to the explicit treatment of all the atoms in a protein, an extended atom model has been developed in which hydrogen atoms are merged with the heavier atoms to which they are bonded, eliminating numerous degrees of freedom. The resultant pseudo-atom is heavier in mass and has a slightly larger van der Waals radius. This is often applied only to hydrogens which cannot potentially hydrogen bond (Brooks et al., 1983).

Despite such simplifying strategies, the simulation of even small proteins for as little as 1 ns is presently intractable. This brief time scale of present molecular dynamics simulations generally precludes direct comparison between simulation results and experimental data, leaving the validity of computational simulations difficult to assess.

We have chosen to examine the motions of the single-tryptophan residue in RNAse-T1 with various simulation strategies using the predicted fluorescence anisotropy decay from each simulation as a measure of its validity. Measures of the limiting anisotropy of indole compounds (Weber, 1960; Valeur and Weber, 1977; Ghiron and Longworth, 1979) and RNAse-T1 (Lakowicz et al., 1983; Eftink, 1983) are available and indicate that the residue is virtually immobilized within its protein matrix. This serves as a rather stringent criterion of accuracy for molecular dynamics simulations since motions in excess of the limited motions detected experimentally should not occur. We report results derived from several types of simulations.

METHODS

Computation

Computations and analyses were performed locally on a Microvax II (Digital Equipment Corp., Marlboro, MA) operating VMS v.4.4 and at the Minnesota Supercomputer Center on a Cray 2 (Cray Research Inc., Mendota Heights, MN) operating Unicos v.2.0, both running the molecular mechanics program CHARMM (Brooks et al., 1983). Graphics were generated using HYDRA by R. Hubbard. Solvent-accessible surface areas were calculated using MS by M. Connolly (Connolly, 1983). HYDRA and CHARMM version 20 were supplied by Polygen (Boston, MA). The parameter and topology files used are identical to those subsequently issued in May 1987 by Polygen, (available from Polygen upon request). Most of the figures contained herein were generated using PLT2 by D. States, et al.

Vacuum Data Sets and Dynamics

X-ray crystal coordinates for ribonuclease-T1 (RNAse-T1) with bound 2′-guanylic acid were kindly supplied by Dr. F. Saenger (Heinemann and Saenger, 1972). Coordinates for the bound ligand were deleted from the dataset in all calculations described below. Coordinates for hydrogen atom positions were generated using CHARMM topology files to yield an EXPLICIT-H dataset with all hydrogens placed (1,454 atoms), and a POLAR-H dataset which included only those hydrogens capable of hydrogen bonding (949 atoms). It was also necessary to generate coordinates for the entire side chain of LYS-41 in both datasets as these were missing from the x-ray data, presumably due to local disorder in the crystal.

Before the calculation of the vacuum trajectories, EXPLICIT-H and POLAR-H datasets were energy-minimized using the adopted-basis Newton-Raphson (ABNR) procedure. Since CHARMM builds hydrogen positions de novo, energy minimization was performed in two steps: initially with movable hydrogens and fixed heavy atoms, then subsequently with heavy atoms released. The initial stage was continued until energy changes for the entire system were < 0.1 kcal/mol/50 steps. The latter stage was continued for 1,000 steps. Bond lengths to hydrogen atoms were constrained at this point by the SHAKE algorithm (Ryckaert et al., 1977; van Gunsteren and Berendsen, 1977) and the structures were heated to 300° K over 1,500 fs.

For purposes of equilibration, velocities were reassigned every 100 fs for 2,000 fs and then scaled every 100 fs for 2,000 fs for temperatures out of the range 290–310° K. Vacuum dynamics trajectories were calculated from this point. In all cases the Verlet algorithm was applied (Verlet, 1967), the step size was 1 fs and coordinate sets were stored every 20 steps. Hydrogen bond terms were not evaluated. The cutoff distance for computing nonbonded interactions was 8.0 Å and lists of such interactions were updated every 20 fs. Initial simulations used a constant dielectric of 1.0, although some later calculations used values of 4.0 or 80.0, or a distance-dependence dielectric as described below. The CHARMM shift function was used in all cases to smooth the transition at the nonbond cutoff distance.

Solvated Data Sets

Starting coordinates for a sphere of water molecules were prepared from a periodically repeated cubic box of 216 TIP3 water models (Jorgenson, 1981) which had been equilibrated, adjusted to a density of 0.0334 molecules $Å^{-3}$, and translated to center on the origin of the coordinate system. Using HYDRA, the coordinates of the EXPLICIT-H and POLAR-H datasets were translated such that residues comprising the two major secondary structures in the vicinity of TRP-59 (loop 60–77 and helix 12–29) were positioned entirely within a 16 Å radius of the same origin (Fig. 1). The water sphere and RNAse-T1 datasets were then

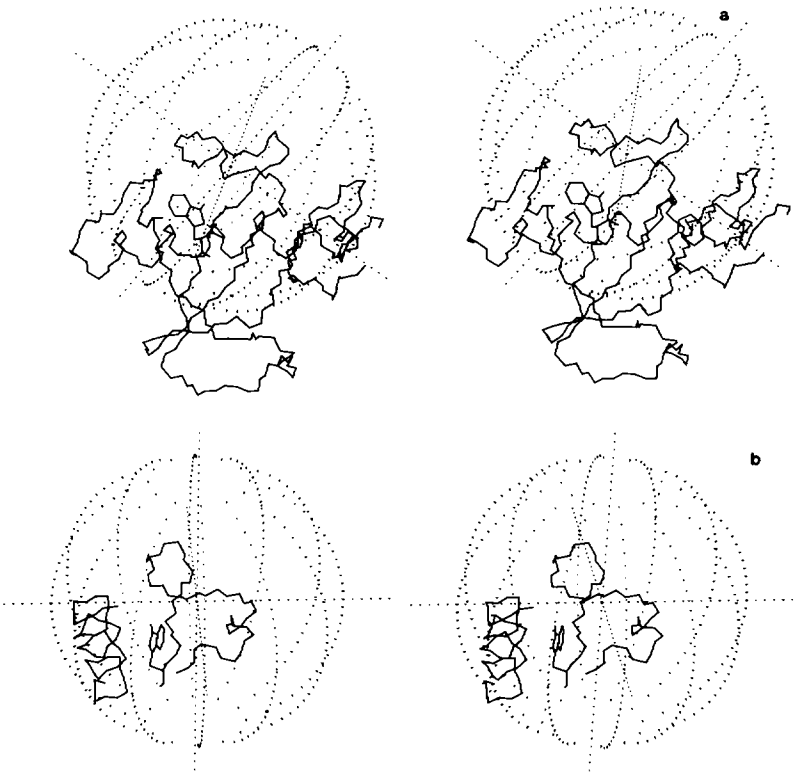

FIGURE 1 Stereo diagrams of TRP-59 and backbone atoms of RNAse-T1 with relative position of stochastic boundary indicated. (*a*) All backbone atoms. (*b*) Backbone atoms only of residues 12–29 (helix) and residues 59–77 (*loop*).

combined and TIP3 molecules in which the oxygen atoms overlapped nonhydrogen protein atoms were deleted. This procedure was arbitrarily repeated 12 times, each time with a different rotational orientation of the water sphere so that cavities large enough to accommodate water molecules were filled.

Partitioning and Design of the Solvated System

The resulting dataset was partitioned according to distance from the coordinate origin. All atoms beyond 16 Å were deleted unless directly connected to an otherwise unbound atom in the buffer region. Atoms between 14 and 16 Å were designated buffer region atoms. A test of connectivity was made to ensure that all atoms within 14 Å of the origin were at least indirectly connected to buffer region atoms. Isotropic harmonic constraints for buffer region protein atoms were derived from atomic root-mean-square (RMS) fluctuations in a 0.5 ps vacuum trajectory according to $k_i = \frac{1}{2}(k_B T/\langle \Delta x_i^2 \rangle)$ where k_i is a constant applied to the square of the displacement of an atom from its reference position, T is the Kelvin temperature, k_B is the Boltzmann constant, and $\langle \Delta x_i^2 \rangle$ is the mean square displacement of the i^{th} atom from its average position. Average values for these constraints are as follows (kcal/mole/Å^2):

	POLAR-H	EXPLICIT-H
α carbon	5.06	7.25
peptide carbon	2.86	10.78
peptide nitrogen	3.41	8.03
side chain heavy atoms	2.33	4.65

A friction coefficient of 100 ps^{-1} was assigned to all heavy protein atoms. Water oxygens were assigned to a coefficient of 62 ps^{-1} and coefficients for all hydrogen atoms were set to zero. In order to minimize interfacial effects, both harmonic constraints and friction coefficients were scaled for exposure using the following formula (derived from the switching function given in Brooks, et al., 1983):

$$S(R) = \frac{1}{2}\frac{(R - R_{ON})^2 (3R_{OFF} - R_{ON} - 2R)}{(R_{OFF} - R_{ON})^3},$$

where $R_{ON} = 14.0$, $R_{OFF} = 16.0$, and R is the distance of an atom from the center of the reaction sphere. In practice, this was applied in discrete increments per the following table.

Distance from origin	Factor
14.0–14.5	0.08
15.5–15.0	0.25
15.0–15.5	0.42
15.5–16.0	0.50

The solvent boundary force for a 16 Å system was numerically calculated according to the mean field force approximation of (Brooks and Karplus, 1983). Thus, our solvated simulations closely follow the stochastic boundary molecular dynamics approach of Brooks, et al. (1985). Before calculating a dynamics trajectory, the system was subjected to partial energy minimization using a steepest descent algorithm (10 steps) and the adopted-basis Newton-Raphson procedure (100 steps).

Dynamics of the Solvated System

Dynamics trajectories were calculated using Langevin dynamics for buffer region atoms with friction coefficients and harmonic constraints applied. The standard Verlet algorithm was applied to atoms within 14 Å of the origin. As with vacuum simulations, the step size was 1 fs and datasets were stored every 20 steps. After energy minimization, bond lengths to hydrogen atoms were constrained with SHAKE. Lists of atoms with nonbonded interactions and atoms within the buffer region were updated every 20 steps. Velocities were rescaled every 100 steps for temperatures outside of the range 290–310 K during equilibration

periods. As above, a constant dielectric of 1.0 was used along with the shift function and a nonbonded interaction cutoff of 8.0 Å.

Calculation of Fluorescence Anisotropy Decay

The decay of anisotropy, r, as a function of time is calculated using the average second order Legendre polynomial, $\langle P_2 \rangle$, of the cosine of the angle between absorption and emission dipole moments (Wallach, 1967; Levy and Szabo, 1982). In a molecular dynamics simulation, a term for overall protein motion is not necessary, and the ensemble average must be estimated from a time average of discrete datasets over the course of the simulation (Ichiye and Karplus, 1983).

Thus,

$$r(t_m) = \frac{2}{5} \langle P_2[\hat{\mu}_a(0) \cdot \hat{\mu}_e(t_m)] \rangle$$

$$= \frac{2}{5} (N - m)^{-1} \sum_{n=1}^{N-m} P_2[\hat{\mu}_a(t_n) \cdot \hat{\mu}_e(t_n + t_m)],$$

where N is the number of datasets in the simulation, t_n is the time coordinate of the n^{th} dataset and t_m is the time interval equal to m dynamics time steps. μ_a and μ_e are normalized vectors oriented along the absorption and emission dipole moments, and

$$P_2[\hat{\mu}_a \cdot \hat{\mu}_e] = \frac{3[\hat{\mu}_a \cdot \hat{\mu}_e]^2 - 1}{2}.$$

The function $r(t)$ is generally not calculated for times greater than one half the length of the trajectory.

The long axis of the indole side chain was defined as the vector drawn from the midpoint between atoms $C_{\eta 2}$ and $C_{\zeta 3}$ to atom $C_{\delta 1}$. The short axis was defined as the vector from $C_{\delta 2}$ to $C_{\epsilon 2}$. To obtain rotated dipole moment vectors, the long axis vector was rotated in a plane defined by the long and short axis vectors, using the convention that an orientation along the long axis pointing toward $C_{\delta 1}$ is 0° and rotation to +90° points from $C_{\epsilon 2}$ toward $C_{\delta 2}$.

RESULTS

Tryptophan Topology and Dynamics

Vacuum simulations of an isolated tryptophan molecule brought to our attention a problem involving out-of-plane bending behavior of the indole moiety. Surprisingly, we observed dramatic angulation of the ring planes, often >35°. Energy minimization of isolated TRP brought the structure to a planar saddle-point of the energy surface, but the global minima were in fact structures with rings bent 17° out-of-plane.

The problem was found to be that angle parameters were assigned for atoms C_γ-$C_{\delta 2}$-$C_{\epsilon 3}$ and $N_{\epsilon 1}$-$C_{\epsilon 2}$-$C_{\zeta 2}$ such that the sum of angles around atoms $C_{\delta 2}$ and $C_{\epsilon 2}$ were both <360°. Specific deletions of these parameters is possible within CHARMM. TRP dynamics following such deletions show far more planar indole ring dynamics with root-mean-square out-of-plane angle fluctuations reduced in vacuo from 11° to 3° (EXPLICIT-H topology). All resulting structures had planar minimum-energy configurations. After such deletion, vibrational analysis of TRP normal modes yielded good agreement with published vibrational spectrum data when using EXPLICIT-H topology (see Table I). Somewhat lesser agreement is obtained using POLAR-H topology.

Description of Crystal and Energy-minimized Structures

Five large elements of secondary structure are apparent on examination of the RNAse T1 crystal structure. There are 17 residues in an α-helix, a twisted antiparallel β-sheet with a β-bulge, and three large loops resembling omega loops (Leszczynski and Rose, 1986). TRP-59 is part of the b-sheet with its side chain situated in a narrow cleft between the helix and one of the omega loops (residues 60–77). There is little apparent room for motional excursions due to close proximity with residues ALA-19 and ALA-22 of the helix, the carbonyl oxygen of PRO-60, and the edge aspect of TYR-68 (Fig. 2).

Solvent-accessible surface areas (defined as by Connolly, 1983) differ somewhat depending on the topology used. With the POLAR-H topology, two separate areas are accessible to a 1.4 Å probe; one associated with atoms $C_{\zeta 2}$ and $C_{\eta 2}$ of the six-atom ring and another smaller area associated with the $H_{\epsilon 1}$ atom of the five-atom ring (see Table II). The side chain of a single residue, VAL-67, is positioned superficial to the TRP-59 side chain and separates these two accessible surfaces.

The accessible surface of the five-atom ring in the POLAR-H model is actually the base of a small pit in the protein surface which has the overall dimensions of a water molecule. In the EXPLICIT-H dataset, this latter surface is not accessible to a 1.4 Å probe from the protein surface, but the dimensions of the cavity remain sufficient to contain a water molecule.

The nucleic acid binding site is on a side of the protein opposite to TRP-59. Although the side chain of the adjacent GLU-58 is involved with nucleic acid binding and endonuclease activity, this side chain is oriented directly

TABLE I
VIBRATIONAL FREQUENCIES (Hz) FOR INDOLE AND INDOLE DERIVATIVES

	Propellor mode	Butterfly mode
Indole (experimental)*	207	240
(experimental)‡	224	254
(calculated)§	205	221
Indole (EXPLICIT-H)	207	230
Skatole (POLAR-H)	64	150
(EXPLICIT-H)	176	268
Tryptophan (EXPLICIT-H)	233	261

Data cited from the literature: *Lautié et al., 1980; ‡Smithson et al., 1984; Note: The descriptive assignment of modes from both these sources is uncertain; §Weiner et al., 1986. The last reference clearly illustrates both modes. Original data were calculated using the VIBRAN utility with CHARMM and were assigned after visualizing the mode trajectory using HYDRA. Molecular structures generated by CHARMM using the indicated topology were exhaustively energy-minimized before analysis.

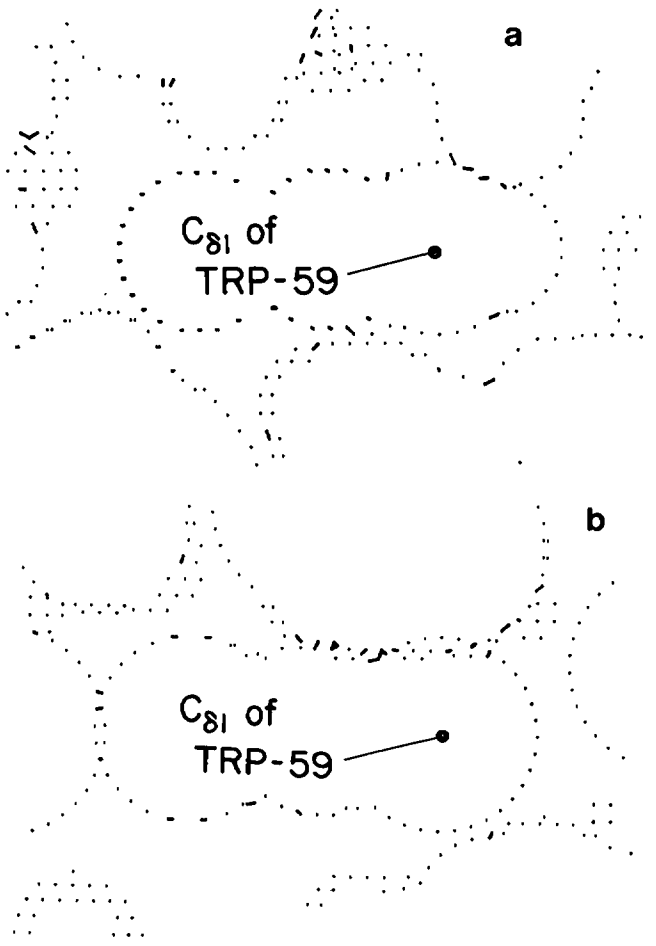

Figure 2 Packing of TRP-59 side chain in RNAse-T1. Cross sections of the VDW surface perpendicular to the plane of the rings and parallel to the long axis are shown. (*a*) EXPLICIT-H model, (*b*) POLAR-H model.

opposite to that of TRP-59 and the substrate binding site is ~12 Å away from the TRP side chain.

RMS differences between minimized and crystal datasets using EXPLICIT-H topology are shown in Fig. 3 *a*. The overall RMS difference was 1.44 Å; main and side chain contributions were 1.03 and 1.61 Å, respectively.

TABLE II
SOLVENT-ACCESSIBLE SURFACE AREAS (Å²) of TRP FOR THE X-RAY CRYSTAL STRUCTURES OF RNAse-T1:

Topology type	Ring	Contact	Reentrant	Total
POLAR-H	5-atom	0.0	4.7	4.7
	6-atom	1.3	11.3	12.6
	Both	1.3	16.0	17.3
EXPLICIT-H	5-atom	0.0	0.0	0.0
	6-atom	0.9	11.3	12.2
	Whole protein	1441.0	3231.2	4672.3

Surface areas calculated by the use of MS (Connolly, 1983) with accompanying parameter files and a 1.4 Å probe sphere. Hydrogen positions were exhaustively energy-minimized in both topologies.

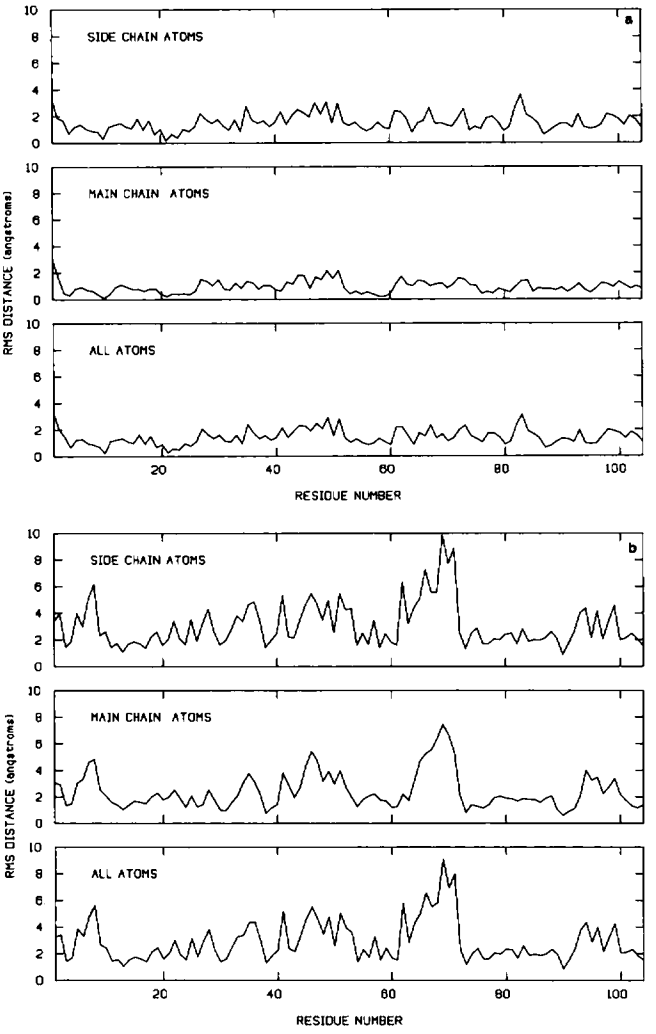

FIGURE 3 Atomic displacements between coordinate sets expressed as the root-mean-square (RMS) positional difference between coordinate sets averaged by residue (EXPLICIT-H vacuum simulation). (*a*) Displacements of the energy-minimized coordinates (all positions minimized) from the x-ray crystal structure (only hydrogen positions minimized). (*b*) Displacement of the average atomic position during the dynamics trajectory from the energy-minimized structure.

Results using POLAR-H topology are ~30% larger. Noting that residues 19–23, 39, 60, and 67–69 are closest to TRP-59, it may be seen that crystal structure relationships in the vicinity of TRP-59 are relatively well preserved at this step.

Anisotropy Decay—Vacuum Simulation

The vacuum simulations of RNAse-T1 using both topologies were conducted for 6.0 ps, after minimization, heating, and 4.0 ps of equilibration. The RMS differences between the minimized dataset and the average position during the dynamics trajectories is shown in Fig. 3 *b*. The $\langle P_2 \rangle$ correlation functions for these simulations were calculated assuming colinear absorption and emission dipoles oriented

along the long axis of the TRP-59 side chain. A result not less than 0.94 was sought since this value represents the minimum value of $r(o)$ (RNAse-T1)/r_o(N-acetyl tryptophanamide) observed by Lakowicz et al. (1983). The data shown in Fig. 4 show that the calculated correlation functions decay to <0.90 within 2 ps; i.e., well beyond experimentally observed values. Other orientations for the assumed dipoles generally yielded even greater decays.

The reason for these results was clear upon visual inspection of the simulation using HYDRA. Residues 60–77 comprise a loop which sterically interacts with TRP-59 at multiple points. This loop had withdrawn a substantial distance from TRP-59, increasing the accessible surface area of the residue severalfold and allowing the ring system to rotate unhindered through a relatively large angle.

The movement is reflected in Fig. 3 *b* as a conspicuous set of peaks corresponding to residues 61–70. The driving force for this movement appears to be large and due to multiple electrostatic interactions, chiefly among backbone atoms. As such, it is unlikely to be a periodic event wherein the steric barrier around the TRP would re-form if the simulation was continued for a longer time.

Several attempts to fix this problem by using distance-dependent or constant but higher dielectrics were made. Setting the dielectric equal to the interatomic distance or raising it from 1.0 to either 4.0 or 80.0 slowed movement of the loop away from the TRP and supports our impression that electrostatic interactions drive this movement. Nevertheless, critical residues adjacent to TRP-59 were eventually displaced to a degree that allowed a decay of anisotropy which was significantly in excess of measured values.

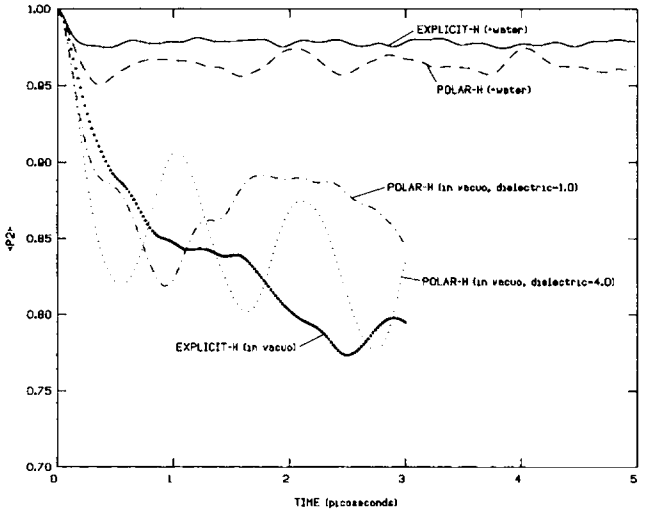

FIGURE 4 Average value of $P_2(t)$ for the indicated simulations. The function was calculated from 5.5 to 11.5 ps in the vacuum simulations and from 10.0 to 20.0 ps in the solvated simulations. The vectors $\hat{\mu}_a$ and $\hat{\mu}_r$ were colinear and parallel to the long axis of the indole rings.

Anisotropy Decay—Solvated Simulations

We further attempted to improve the correlation between simulated and measured anisotropy decay by adding water to the simulation. A 16 Å spherical stochastic boundary was positioned such that the two major secondary structures bounding TRP-59 (loop 60–77 and helix 12–29) were entirely contained within the boundary. Protein atoms within the buffer region between 14 and 16 Å from the center of the sphere were constrained as described above and atoms beyond 16 Å were deleted. TIP3 water molecules were added as described in the Methods. The resulting system contained 204 water molecules and either 636 (POLAR-H) or 998 (EXPLICIT-H) protein atoms. Total system energy as a function of time is shown in Fig. 5. This figure indicates that a substantial amount of energy is dissipated through the boundary in the first 10 ps of both simulations. Accordingly, data from the first half of each simulation are not used in subsequent calculations in order to study the system in as fully an equilibrated state as possible. The average temperature was 300.1°C and 300.3°C for POLAR-H and EXPLICIT-H simulations, respectively.[2]

The addition of solvent improved the agreement between simulation and experiment dramatically. As shown in Fig. 4, simulations using either topology appear to yield a plateau value of $\langle P_2 \rangle = 0.96$ within one ps, in excellent agreement with experimental measurement. The results correspond to finding that gross movements of the residue 60–77 loop do not occur as in the vacuum simulation. In order to rule out the possibility that some feature of the solvated system other than explicit water prevented such movement, the system was also propagated with water deleted. In this case, movement of the residue 60–77 loop occurs at a similar rate and to a similar extent as in the aforementioned vacuum simulations, despite the atom deletions, constraints and friction coefficients that were part of the solvated system.

The above result applies only to the case of colinear

[2]Since completion of the simulations in which a preliminary solution to the crystal structure was used, a coordinate set derived from slightly higher resolution data has been deposited in the Brookhaven Protein Data Bank. In these refined data residue 25 was changed from LYS to GLN, and residues 71–73 were changed from PRO-GLY-SER to GLY-SER-PRO. Since it seemed possible that these changes could explain the movement of residues 60–77 and consequently, the unacceptably large anisotropy decay in our vacuum simulations, we conducted a POLAR-H vacuum simulation using these refined coordinates (950 atoms) under identical circumstances to that of the above reported calculation (949 atoms). This new simulation also exhibited a movement of residues 60–77 away from TRP-59 and a similarly large anisotropy decay. Since the locations of residue changes are remote to the vicinity of principal interest (the TRP-59 side chain), and such changes do not correct problems we encountered in our relatively brief vacuum simulations, we chose to continue the analysis of our original trajectories rather than also repeat our larger solvated simulations with the new primary sequence and refined crystal coordinates.

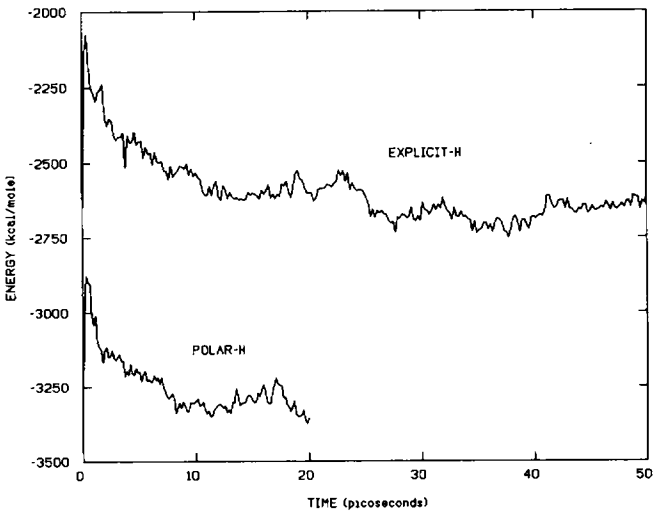

FIGURE 5 Total internal energy of the protein-solvent system during the simulations. Total internal energy is the sum of bonded and nonbonded energy terms plus constraint energies associated with buffer region protein atoms and stochastic boundary forces on the water molecules.

dipole moments oriented along the long axis of the ring system. In reality it is believed that the absorption moment makes an angle of $-38°$ with the long axis (Yamamoto and Tanaka, 1972) and is not colinear with the emission moment. Therefore, to consider more realistic cases, the dipole vectors were individually rotated in a plane defined by vectors parallel to the long and short axes. The plateau value of the $\langle P_2 \rangle$ correlation function was calculated at 10° intervals for the entire range of possible dipole orientations. These results are shown plotted in Fig. 6.

Two features of this figure are worthy of note. First, the plateau value of the $\langle P_2 \rangle$ correlation function for colinear dipoles ranges from a minimum of 0.944 at $-50°$ to a maximum of 0.969 at $+40°$, reflecting rotational cone angles of 11.3° and 8.3°, respectively. Second, as the angle, α, between absorption and emission dipoles increases, the correlation function plateau assumes a nearly constant value regardless of the orientation of the dipoles within the plane of the rings. This finding simplifies the comparison of simulation and experimental results, since the former now may be regarded as virtually independent of assumptions regarding orientation of the dipole pair. Indeed, the plateau values are given to a good approximation by the expression.

$$\langle P_2[\hat{\mu}_a(0) \cdot \hat{\mu}_e t)] \rangle = P_2(\cos \alpha) \langle P_2[\hat{\mu}_a(0) \cdot \hat{\mu}_a(t) \rangle.$$

As discussed by Ichiye and Karplus (1983), the accuracy of this type of expression depends on several assumptions, some of which are rather questionable. Our finding that this approximation is nevertheless accurate supports the use of the foregoing equations in the particular case of RNAse-T1. It follows that the anisotropy decay may be derived with reasonable accuracy from

$$r(t) = r_0 \langle P_2 [\hat{\mu}_a(0) \cdot \hat{\mu}_a(t)] \rangle,$$

where

$$r_0 = \tfrac{2}{5} P_2 (\cos \alpha).$$

Nevertheless, we calculated the value of the $r(t)$ correlation function (from the equation given in Methods) assigning $\mu_a = -38°$ and $\mu_e = -38° \pm \alpha$ for values of α corresponding to reasonable values of r_0. In the solvated simulations, this function quickly reaches a level plateau for all orientations of μ_a and μ_e, and $r(t)$ values for the two different orientations of μ_e are very similar (Fig. 7). For

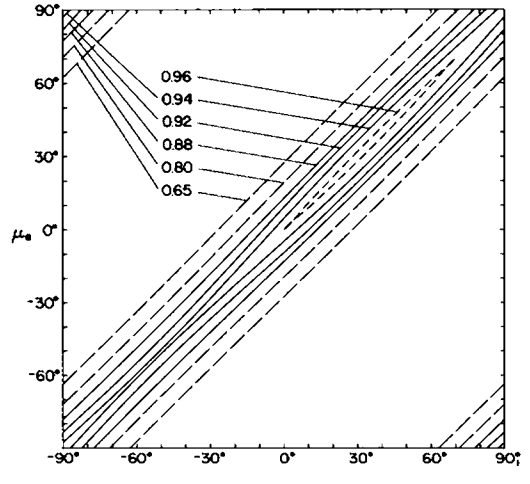

FIGURE 6 Plateau values of $\langle P_2 [\hat{\mu}_a(0), \hat{\mu}_e(t)] \rangle$ for various orientations of μ_a and μ_e in the plane of the rings. Contour levels are drawn for indicated values of $\langle P_2 \rangle$. The plot appears to be symmetric about the $\mu_a = \mu_e$ axis, but in fact this merely reflects the similarity of the correlation function in both the forward and reverse directions.

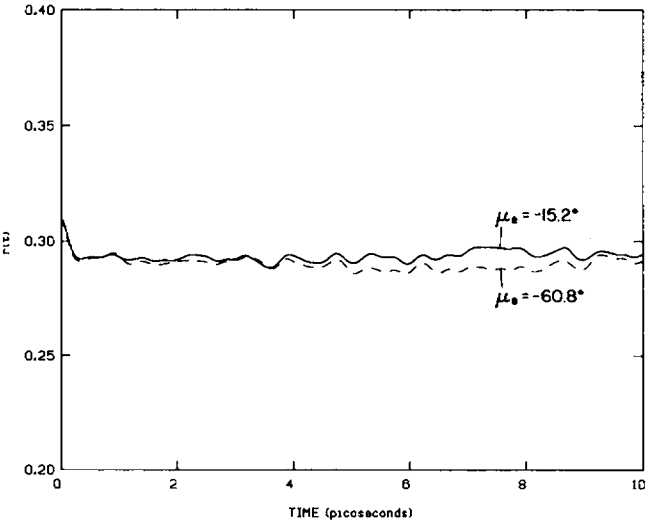

FIGURE 7 Plot of $r(t)$ for the solvated EXPLICIT-H simulation assuming $\mu_a = -38.0°$ and $\mu_e = \mu_a \pm 22.80$ (corresponds to a limiting anisotropy of 0.31).

results listed in Table III, we have listed the plateau values for $r(t)$ using both $r_0 = 0.30$ and 0.31 to illustrate how an uncertainty in this value affects the final results.

DISCUSSION

Several unusual features of tryptophan fluorescence in RNAse-T1—a high limiting anisotropy, a blue-shifted and structured emission spectrum, and differential susceptibility to quenchers—prompt one to look for structural correlations to these phenomena. The x-ray crystal structure, while essential to such work, has not proven sufficient to provide the necessary information. A molecular dynamics simulation of this protein is a logical next step since anisotropy decay may be derived from such calculations in a straightforward manner. Furthermore, comparison of the anisotropy decay predicted by various simulation strategies enables one to estimate the relative accuracy of each simulation in the vicinity of the TRP residue and indicates which strategy is most likely to generate useful correlations with other experimentally observable phenomena.

In the face of limited computational power, molecular dynamics simulations are often conducted with nonpolar hydrogens considered implicitly through the adjustment of nonbonded parameters of the heavy atom to which they are bonded. The latter procedure yields effective molecular volumes somewhat larger than if hydrogens were considered explicitly. For example, a "van der Waals cross section" of a benzene ring through two vertices is ~6% longer and 17% wider using POLAR-H topology than with EXPLICIT-H topology. We would expect the particular case of TRP-59 dynamics to be quite sensitive to the choice of topology since the volume of the cavity containing the indole side chain is only slightly larger than the indole itself. Indeed, the packing of the rings is discernibly different between the two topologies (see Fig. 2).

In the full solvated simulations there is extremely close agreement between simulations using POLAR-H and EXPLICIT-H topologies in terms of predicted anistropy decay. Table III shows that these differences are of smaller consequence than our experimental uncertainty surrounding the limiting anisotropy of indole. We have elected to propagate our EXPLICIT-H simulation the longest in anticipation of studies requiring explicit treatment of volumes and surfaces. Therefore, we find a measure of reassurance in the agreement between the results of this simulation and our POLAR-H simulation since the latter presumably uses more highly developed and extensively tested parameters.

TABLE III
PLATEAU VALUE FOR $r(t)$ IN THE SOLVATED SIMULATIONS

μa	$\mu_e - \mu_a + \alpha$	$r_0 = P_2$	POLAR-H	EXPLICIT-H
		α		
−38.0	−13.9	0.30	0.286	0.289
−38.0	−62.1	0.30	0.280	0.286
−38.0	−15.2	0.31	0.295	0.299
−38.0	−60.8	0.31	0.290	0.296
+40.0	+40.0	0.31	–	0.300
−50.0	−50.0	0.30	–	0.282

Calculations assumed a limiting anisotropy for indole compounds of either 0.30 (corresponding to $\alpha = \pm 20.8$) or 0.31 ($\alpha = 22.8°$). Values for dipole orientations of +40.0 and −50.0 correspond to the maximum and minimum values of $\langle P_2 \rangle$, respectively, as derived for the EXPLICIT-H simulation (see Fig. 6).

The explicit inclusion of solvent in these simulations profoundly affected our results. This is consistent with pervasive solvent-induced effects on protein dynamics noted by other authors (van Gunsteren and Karplus, 1982; Ahlström et al., 1987). We find intriguing the brief description by Brooks and Karplus (1986) of solvent effects on the anisotropy decay of TRP-62 and TRP-63 in lysozyme. These authors report that the presence of solvent caused a slow anisotropy decay in both residues which was not present in a vacuum simulation. Unfortunately, the presence of six TRP residues in this protein precludes an unequivocal correlation of these results with experimental data.

In terms of gross conformational changes, the presence of solvent in our simulations inhibited movement of the loop comprised of residues 60–77. Several of these residues form one wall of the cavity containing the TRP-59 side chain and substantially greater mobility of the side chain is possible if the loop recedes as in our vacuum simulations. The driving force for these movements has not been characterized fully, but preliminary calculations reveal a marked reduction in protein surface charge density and an increase in the number of H-bonds among these residues in the vacuum simulations (data not shown). Movement of the loop in the solvated simulations is inhibited by the presence of water which may stabilize the polar groups involved and thereby reduce or eliminate the driving force for movement. Alternatively, the water may have merely slowed movement of the loop by virtue of mass or friction effects. Late in the simulation we observed that the water had receded away from the boundary in the vicinity of the loop, leaving a small region of unoccupied space between the boundary and the water mass. This finding has two implications. First, boundary forces are not being transmitted to the loop through the water so as to prevent movement of the loop. Second, the pressure of the water within the boundary is neither uniform, constant, nor sufficiently high to mimic an ordinary solvated system. We find this to be a difficult property to simulate using the stochastic boundary technique, since creation of a reasonably stable normobaric solvent partition may require enormous amounts of additional computational effort. For the purpose of the work herein, it seems preferable to have an abnormally low pressure in the solvent region so that a high value for the simulation-derived anisotropy may not be attributable to a high solvent pressure.

Our vacuum simulations invariably predicted anisotropy

decays far in excess of that observed experimentally, and demonstrated as high as 100-fold increases in solvent accessible surface area for TRP-59 (data not shown). We conclude that these simulations do not realistically simulate the environment of TRP-59 and are not suitable for further study of structure-fluorescence correlations. In addition, they preclude an analysis of solvent effects on side chain motion such as performed by Ghosh and McCammon (1987a). These authors found relatively small effects on TYR-35 rotational isomerization in bovine pancreatic trypsin inhibitor (BPTI) upon adding solvent. In subsequent work, (Ghosh and McCammon, 1978*b*) these same authors examined the consequences of changing the viscosity of a solvated system, again finding relatively small effects. Thus, we cannot generalize our findings in RNAse-T1 to imply that the explicit inclusion of solvent is required for the realistic simulation of all proteins. However, the differences between simulations of RNAse-T1 and BPTI do point to the care one must apply in designing a dynamics simulation. In both cases, correlation with experimentally measured data are possible, and such internal standards are a great advantage in estimating the accuracy of any simulation.

MacKerell et al. (1987) have briefly described a 55.5 ps vacuum POLAR-H simulation of RNAse-T1 run at an average temperature of 324 K. These authors assumed an r_0 of 0.31 and report a value ≤ 0.24 for the plateau anisotropy decay. In addition, they report an experimental value of 0.264 for the limiting anisotropy of RNAse-T1 and a biexponential fluorescence intensity decay at pH = 5.3. Extrapolating from our relatively brief POLAR-H vacuum simulations and despite a rather substantial average temperature difference, we find our simulation results entirely concur with these authors. However, these vacuum simulations all in fact indicate an excessively large anisotropy decay. Finding that all of our vacuum simulations predicted such decays after only several picoseconds despite various treatments of the dielectric, we decided not to propagate them further.

Lakowicz et al. (1983) for example, have also reported a limiting anisotropy of 0.264 for RNAse-T1. However, these authors also found that the anisotropy of various indole compounds in vitrified solutions ranged from 0.26 to 0.28. Thus, their value for RNAse-T1 is 0.943 of their maximum for indole and they conclude that the TRP in RNAse-T1 is largely immobilized. Eftink (1983) reached an essentially identical conclusion although he assumed r_0 for indole to be 0.31 ± 0.02 and reported a value for RNAse-T1 of 0.32. We have measured the steady-state anisotropy of RNAse-T1 in 80% glycerol at -50°C and found a value of 0.289 (unpublished results). We suspect this may be a slight underestimate, but in any case, both simulated and experimental anisotropies should be at least as high as this value.

The biexponential decay reported by MacKerell et al. is at variance with the work of other groups who report single exponential decays at pH <6.0 and biexponential decays only at pH ≥7.0 (Grinvald and Steinberg, 1976; James et al., 1985; Chen et al., 1987; Eftink and Ghiron, 1987). The disparity between these results may be related to the relatively high temperature (40°C) used by MacKerell et al. in their experimental studies.

It may be questioned whether existing experimental data are consistent and accurate enough to enable distinction between these simulations, given a rather wide range of values reported for the limiting anisotropy of indole. Furthermore, the experimental determination of $r(o)$ involves anistropy measurements as a function of fluorescence lifetime, and characteristically requires a rather long extrapolation, particularly in the case of RNAse-T1 (Lakowicz et al., 1983; Eftink 1983). However, most published work is in agreement that the limiting anisotropy of RNAse-T1 is the highest of any single TRP protein and implies that the fluorophore is virtually immobile within this protein. An anisotropy decay plateau of 0.24 as reported by MacKerrell (and as supported by our POLAR-H vacuum simulations) represents a decay to 0.77 of their limiting value (0.31) and roughly corresponds to a 23° cone of rotation. This is substantially larger than most other single TRP proteins and approaches that of glucagon (Eftink, 1983). Fig. 4 in the last reference clearly shows that the data are sufficiently precise to assign a much higher limiting anisotropy to RNAse-T1 than to monellin, for example.

There remain at least two unanswered but fundamental questions. First, can an electrostatically inhomogenous protein environment significantly alter the angular orientation of transition moments for the indole moiety? A change in the orientation of either moment by merely a few degrees will markedly affect the outcome of an anisotropy measurement. This points to the need for an independent measure of TRP motion such as by the use of ^{13}C-nuclear magnetic resonance (Weaver, A. J., M. D. Kemple, and F. G. Prendergast, manuscript submitted for publication). Second, how do quenching agents used in the measurement of the limiting anisotropy make effective contact with tryptophan in RNAse-T1? If quenchers such as oxygen and acrylamide require access to the fluorophore other than that access which is evident from the crystal structure (Table II), internal fluctuations must occur which further expose the tryptophan side chain, yet do not permit increased rotational freedom. Movements of residues 60–77 as observed in our vacuum simulations do not appear to meet these criteria.

The authors would like to thank Drs. C. L. Brooks III, B. R. Brooks, and A. Brünger for guidance at various stages of this work; Dr. M. Karplus for version 19 of CHARMM; Dr. W. Saenger for the x-ray coordinates of RNAse-T1; The Minnesota Supercomputer Institute and Mr. R. Walsh for computational support at the Minnesota Supercomputer Center; and Ms. Linda Wilkin, Ms. Patricia Hart, and Mr. Peter Callahan for assistance in preparation of the manuscript.

This work was supported by GM34847 and presented at the meeting of the Biophysical Society, Feb 22–26, 1987. Funds for purchase of the Evans and Sutherland graphics facility were generously provided by the Ahmanson Foundation.

Received for publication 6 November 1987 and in final form 7 March 1988.

REFERENCES

Ahlström, P., O. Teleman, B. Jönsson, and S. Forsen. 1987. Molecular dynamics simulation of parvalbumin in aqueous solution. *J. Am. Chem. Soc.* 109:1541–1551.

Alcala, J. R., E. Gratton, and F. G. Prendergast. 1987. Interpretation of fluorescence decays in proteins using continuous lifetime distributions. *Biophys. J.* 51:925–936.

Berkowitz, M., and J. A. McCammon. 1982. Molecular dynamics with stochastic boundary conditions. *Chem. Phys. Lett.* 90:215–217.

Brooks, B. R., R. E. Bruccoleri, B. D. Olafson, D. J. States, S. Savanirnathan, and M. Karplus. 1983. CHARMM: A program for macromolecular energy minimization and dynamics calculations. *J. Comp. Chem.* 4:187–217.

Brooks III, C. L., and M. Karplus. 1983. Deformable stochastic boundaries in molecular dynamics. *J. Chem. Phys.* 79:6312–6325.

Brooks III, C. L., and M. Karplus. 1986. Theoretical approaches to solvation of biopolymers. *Meth. Enzymol.* 127:369–400.

Brooks III, C. L., A. Brünger, and M. Karplus. 1985. Active site dynamics in protein molecules: a stochastic boundary molecular dynamics approach. *Biopolymers.* 24:843–865.

Brünger, A., C. L. Brooks III, and M. Karplus. 1984. Stochastic boundary conditions for molecular dynamics simulations of ST2 water. *Chem. Phys. Lett.* 105:495–500.

Chen, L. X. Q., J. W. Longworth, and G. R. Fleming. 1987. Picosecond time-resolved fluorescence ribonuclease-T_1. *Biophys. J.* 51:865–873.

Connolly, M. C. 1983. Solvent accessible surfaces of proteins and nucleic acids. *Science (Wash., DC).* 21:709–713.

Creed, D. 1984. The photophysics and photochemistry of the near-UV absorbing amino acids—I. Tryptophan and its simple derivatives. *Photochem. Photobiol.* 39:537–562.

Eftink, M. R. 1983. Quenching-resolved emission anisotropy studies with single and multitryptophan-containing proteins. *Biophys. J.* 43:323–334.

Eftink, M. R., and C. A. Ghiron. 1975. Dynamics of a protein matrix revealed by fluorescence quenching. *Proc. Natl. Acad. Sci. USA.* 72:3290–3294.

Eftink, M. R., and C. A. Ghiron. 1987. Frequency domain measurements of the fluorescence lifetime of ribonuclease T_1. *Biophys. J.* 52:467–473.

Gelin, B. R., and M. Karplus. 1975. Side-chain torsional potentials and motion of amino acids in proteins: Bovine pancreatic trypsin inhibitor. *Proc. Natl. Acad. Sci. USA.* 72:2002–2006.

Ghiron, C. A., and J. W. Longworth. 1979. Transfer of singlet energy within trypsin. *Biochemistry.* 18:3828–3832.

Ghosh, I., and J. A. McCammon. 1987a. Side-chain rotational isomerization in proteins. *Biophys. J.* 51:637–641.

Ghosh, I., and J. A. McCammon. 1987b. Solvent viscosity effects on the rate of side-chain rotational isomerization in a protein molecule. *J. Phys. Chem.* 91:4878–4881.

Grinvald, A., and I. Z. Steinberg. 1976. The fluorescence decay of tryptophan residues in active and denatured proteins. *Biochim. Biophys. Acta.* 427:663–678.

Heinemann, U., and W. Saenger. 1982. Specific protein-nucleic acid recognition in ribonuclease T_1-2′-guanylic acid complex: an x-ray study. *Nature (Lond.)* 299:27–31.

Ichiye, T., and M. Karplus. 1983. Fluorescence depolarization of tryptophan residues in proteins: a molecular dynamics study. *Biochemistry.* 22:2884–2893.

James, D. R., D. R. Demmer, R. P. Steer, and R. E. Verrall. 1985. Fluorescence lifetime quenching and anisotropy studies of ribonuclease T_1. *Biochemistry.* 24:5517–5526.

Jorgensen, W. L. 1981. Transferable intermolecular potential functions for water, alcohols, and ethers. Application to liquid water. *J. Am. Chem. Soc.* 103:335–340.

Lakowicz, J. R., G. Laczko, and I. Grycynski. 1987. Picosecond resolution of tyrosine fluorescence and anisotropy decays by 2-GHz frequency-domain fluorometry. *Biochemistry.* 26:82–90.

Lakowicz, J. R., B. P. Maliwal, H. Cherek, and A. Balter. 1983. Rotational freedom of tryptophan residues in proteins and peptides. *Biochemistry.* 22:1741–1752.

Lautié, A., M. F. Lautié, A. Gruger, and S. A. Fakhri. 1980. Etude par spectométrie i.r. et raman de l'indole et de l'indolizine. Liaison hydrogine NH . . . p*. *Spectrochim. Acta. Part A Mol. Spectrosc.* 36A:85–94.

Leszczynski, J. F., and G. D. Rose. 1986. Loops in globular proteins: a novel category of secondary structure. *Science (Wash., DC).* 234:849–855.

Levy, R. M., and A. Szabo. 1982. Initial fluorescence depolarization of tyrosines in proteins. *J. Am. Chem. Soc.* 104:2073–2075.

MacKerell, A. D. Jr., R. Rigler, L. Nilsson, U. Hahn, and W. Saenger. 1987. Protein dynamics study of ribonuclease—T_1. *Biophys. Chem.* 26:247–261.

McCammon, J. A., and S. C. Harvey. 1987. Dynamics of proteins and nucleic acids. *Cambridge University Press.*

Ryckaert, J. P., G. Liccotti, and H. J. C. Berendsen. 1977. Numerical integration of the cartesian equations of motion of a system with constraints. Molecular dynamics of n-alkanes. *J. Comp. Phys.* 23:327–343.

Smithson, T. L., R. A. Shaw, and H. Wieser. 1984. The vapor phase far-infrared spectra of 1H-indene, benzo[b]furan, 1,3,2-benzodioxaborole and indole. *J. Chem. Phys.* 81:4281–4287.

Valeur, B., and G. Weber. 1977. Resolution of the fluorescence excitation spectrum of indole into the ^1L_a and ^1L_b excitation bands. *Photochem. Photobiol.* 25:441–444.

van Gunsteren, W. F., and H. J. C. Berendsen. 1977. Algorithms for macromolecular dynamics and constraint dynamics. *Mol. Physiol.* 34:1311–1315.

van Gunsteren, W. F., and M. Karplus. 1982. Protein dynamics in solution and in a crystal environment—a molecular dynamics study. *Biochemistry.* 21:2259–2274.

Verlet, L. 1967. Computer "experiments" on classical fluids. I. Thermodynamic properties of Lennard-Jones molecules. *Phys. Rev.* 159:98–103.

Wallach, D. 1967. Effect of internal rotation on angular correlation functions. *J. Chem. Phys.* 47:5258–5268.

Weber, G. 1960. Fluorescence-polarization spectrum and electronic-energy transfer in tyrosine, tryptophan, and related compounds. *Biochem. J.* 75:335–345.

Weiner, S. J., P. A. Kollman, D. T. Nguyen, and D. A. Case. 1966. An all atom force field for simulations of proteins and nucleic acids. *J. Comp. Chem.* 7:230–252.

Yamamoto, Y., and J. Tanaka. 1972. Polarized absorption-spectra of crystals of indole and its related compounds. *Bull. Chem. Soc. Jpn.* 45:1362–1366.